IEEE Access
Multidisciplinary | Rapid Review | Open Access Journal

Received July 5, 2019, accepted July 16, 2019, date of publication July 29, 2019, date of current version August 21, 2019.

Digital Object Identifier 10.1109/ACCESS.2019.2931767

Study of Fuel-Controlled Aircraft Engine for Fuel-Powered Unmanned Aerial Vehicle: Energy Conversion Analysis and Optimization

YIXUAN WANG[1], YAN SHI[1], MAOLIN CAI[1], WEIQING XU[1], TIANYU PAN[2], AND QIHUI YU[3]

[1]School of Automation Science and Electrical Engineering, Beihang University, Beijing 100191, China
[2]School of Energy and Power Engineering, Beihang University, Beijing 100191, China
[3]Department of Mechanical Engineering, Inner Mongolia University of Science and Technology, Baotou 014000, China

Corresponding author: Yan Shi (yesoyou@gmail.com)

This work was supported in part by the National Natural Science Foundation of China under Grant 51605013.

ABSTRACT Recently, the cruising duration is a vital parameter of fuel-powered unmanned aerial vehicles (UAVs), and it is directly determined by the power characteristics of the aircraft engine in the UAV. In this study, to prolong the flight duration and enhance the power and efficiency of a UAV, an aircraft engine is analyzed based on the fuel injection control system and output power characteristics. First, the mathematical model of a fuel-controlled engine is constructed. In addition, the experimental stations of the aircraft engine are set up to verify the mathematical model. Furthermore, the effects of key parameters on the engine power characteristics are examined. By the experimental and simulation studies validity of the mathematical model is effectively verified which indicates that the increased rotating speed decreases the power efficiency of the aircraft engine, and reducing the fuel injection pulse width from 5 ms to 3.5 ms increases the power efficiency by 10%. Moreover, increasing the advance angle of ignition from 10° to 40° improves the power efficiency by 5%. In addition, when the fuel injection delay width increases from 0.5 mm to 1.5 mm at an engine speed between 3500 rpm and 4000 rpm, the power efficiency is improved by 6%. Finally, when the engine speed is higher than 4000 rpm, increasing the propeller rotor diameter from 650 mm to 800 mm enhances the power efficiency of the aircraft engine by approximately 5%. This research can be considered as the fuel injection system optimization and cruising duration improvement of a fuel-powered UAV.

INDEX TERMS Aircraft engine, fuel injection control system, power characteristics, efficiency, fuel-powered unmanned aerial vehicle.

I. INTRODUCTION

Recently, fuel-powered unmanned air vehicles (UAVs) have been widely applied in agriculture, plant protection, transportation, and field surveillance due to their simple structure, easy control, steady running, and landform independence [1]–[5]. The cruising duration has gradually become a key technical indicator to evaluate the UAV performance since a short cruising duration will limit the UAV application for long-distance flights. Presently, the cruising duration of a typical small UAV is less than 1 h [6], [7], which cannot satisfy the requirements of long-duration missions.

The associate editor coordinating the review of this manuscript and approving it for publication was Tao Wang.

As UAVs can only carry a limited amount of fuel, the cruising duration of a fuel-powered UAV is directly affected by the fuel consumption rate of the aircraft engine. The engine combustion efficiency can be improved and the cruising duration can be prolonged by using a fuel supply optimal control technology. Therefore, increasingly, scientists and engineers have paid attention to fuel control technologies for fuel-powered UAVs [8]–[12].

The aircraft engine, as the power unit of a fuel-powered UAV, is the main study object of a fuel control technology. Most recent studies on the UAV aircraft engine have mainly focused on the structure design and fuel control logic. Lu [13] has conducted research on a two-stroke aircraft engine for a fuel-powered UAV. He obtained the relationship between the output engine power and propeller pulling

force from experiments and calculations. However, the fuel consumption analysis was lacked. Hooper et al. [14] have presented the methods of cold starting a UAV engine based on the experimental experience. In addition, his team [15] has independently conducted aircraft engine modelling to improve the power efficiency. However, in their research, the power efficiency was not optimized. Hasan et al. [16] have studied a diesel engine-powered electrical generator by a series of experiments. They obtained the variations in different gas emissions with the engine power. Furthermore, Pankaj et al. [17] analyzed the effects of a bio-fuel of different proportions on a single cylinder, and confirmed that a dual fuel blend can be a promising source of biodiesel production. But there is still a lack of the aircraft engine model analysis for a fuel-powered UAV, causing difficulty in the optimization of the engine power characteristics.

The studies on aircraft engine modelling are mainly based on fuel-controlled vehicles on the ground [18]–[21]. Yong et al. [28] simulated a diesel engine using a dynamic thermodynamics model, and accurately obtained the simulation results of the engine speed, power, and thermal efficiency. Shamekhi et al. [29] improved the mean value model by using neural networks based on a thermodynamics model. Furthermore, they calculated the pollutant emissions precisely. However, the thermodynamics modeling is highly dependent on the business software, and the calculation time is extremely long [21]. Therefore, numerous research studies adopted mean value modeling methods owing to its advantages of a simple structure and real-time accuracy [18]–[20], [29]–[31]. By using a non-dimensional analysis and singular perturbation techniques, Broomhead [30] updated the mean value model, and he verified the accuracy of the improved models from the experimental data. Kamyar et al. [31] investigated a new block-oriented modeling method to predict the engine performance and emissions. However, model research on an entire UAV power unit is still lacking. In addition, the recent studies have not investigated fuel injection control, which is not advantageous for the optimization of aircraft engine power characteristics.

In this study, to improve the power efficiency of an aircraft engine and extend the cruising duration of a fuel-powered UAV, the power characteristics of a fuel-controlled aircraft engine are examined. Firstly, a mathematical model of the aircraft engine with a fuel control system is constructed. Secondly, the experimental station is set up for the model verification. In addition, the provided fuel process is analyzed based on the simulation results, and then the effect of several key parameters on the power characteristics is studied. This research can be considered as the power characteristic optimization and cruising duration improvement of a fuel-powered UAV.

II. WORKING PRINCIPLE AND FUEL INJECTION CONTROL METHOD OF FUEL-POWERED AIRCRAFT ENGINE

A fuel-powered aircraft engine is electronic fuel injection (EFI)-modified to realize accurate fuel supply control during engine operation. From Fig. 1, the fuel-controlled aircraft engine is mainly composed of two capacitor discharge ignitions (CDIs) and one EFI unit, opposed engine cylinders, Hall sensor, throttle plate controlled by a steering-engine, starting motor, UAV propeller, and assorted engine control unit (ECU).

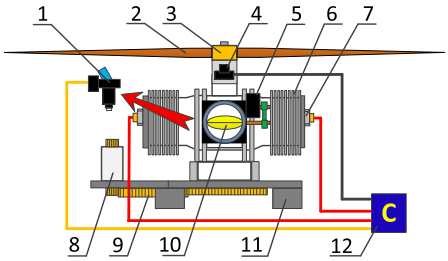

FIGURE 1. Diagram of the structure of a fuel-controlled aircraft engine of a fuel-powered UAV (1) EFI unit, (2) UAV propeller, (3) rotating shaft, (4) Hall sensor, (5) steering-engine, (6) engine cylinder block, (7) CDI ignition, (8) starting motor, (9) multistage transmission gear, (10) throttle plate, (11) engine pedestal, and (12) ECU unit.

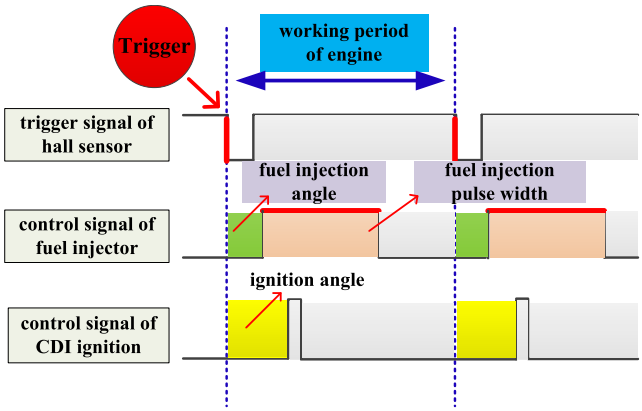

FIGURE 2. Diagram of the fuel injection control principle.

The fuel injection control principle of the aircraft engine is as shown in Fig. 2. The main components in the fuel injection control system include the Hall sensor, fuel injector, and CDI ignition. A magnet is installed on the rotating shaft at 10–30° before the pistons reach the top dead center. When the crankshaft rotates, the hall sensor is triggered, and the fuel injector starts to work. Then the ECU unit calculates the fuel injection angle, pulse width, and ignition angle based on the rotating speed, intake pressure, and other parameters. Some recent works on fuel-powered engines also use an intake pressure sensor, intake flow sensor, and air–fuel ratio analyzer [21], [22]. However, these devices will increase the load of a UAV. Therefore, the control parameters of an aircraft engine are usually set up based on previous experimental results.

III. MATHEMATICAL MODELING OF AIRCRAFT ENGINE BASED ON INJECTION FUEL CONTROL

Studies on fuel-powered engines have been undergoing for several decades [26], [27]. As the foundation of engine

research, the mean value model theory was first proposed by Rasmussen. Elbert Hendricks et al. improved it theoretically and experimentally [18]–[20]. Compared with a traditional thermodynamics model, the mean value model is simple and practical, and various research studies have applied the theory to the engine control. In this study, the EFI working model, engine model, and UAV propeller model are first built.

The magnetic flux formulas when a fuel injector is electrified and not electrified are as follows:

$$U_0 = Ri + N\frac{d\Phi_b}{dt}, \text{ when electrified,} \tag{1}$$

and

$$0 = (R + R_0)i + N\frac{d\Phi_b}{dt}, \text{ when not electrified,} \tag{2}$$

where R is the basic resistance of the electrified coil loop, R_0 is the protective resistance, Φ_b represents the total magnetic circuit, N is the number of the coils, i is the current in the loop, and U_0 is the driving voltage. In addition, the electrified condition means that the control signal is at up level, which the driving voltage can actuate the electric needle valve; the not electrified condition is that when the signal is at low level, the driving voltage instantly loses the electricity which can make the valve closed. The electromagnetic force on the needle valve when the coil is electrified is as follows:

$$F_m = \frac{\mu_0 (iN)^2 S}{2\delta^2}, \tag{3}$$

where μ_0 represents the permeability of vacuum, S is the cross-section of the air gap, and δ represents the length of the working air gap.

The kinetic equations of the magnetic needle valve are as follows:

$$F_m - F_0 - kx + F_{fuel} = m_v \frac{d^2x}{dt^2}, \tag{4}$$

where F_0 is the initial tension of the spring, k is the spring stiffness, x is the displacement of the needle valve, m_v is mass of the needle valve, and F_{fuel} is the pressure of the fuel.

When the needle valve is opened, a high-pressure fuel releases, generating a fuel flow. The equation of the fuel flow is as follows:

$$\dot{m}_{fi} = \mu_n S_n \sqrt{2g\rho_f (p_f - p_m) t_d}, \tag{5}$$

where $\dot{m}_{fi}$ is the mass flow of the input fuel during a single injection, μ_n is the flow coefficient of the injector, S_n is the hole area of the injector, ρ_f represents the density of the fuel, p_f is the fuel pressure, p_m is the manifold air pressure of the engine, and t_d is the open time of the injector. In the engine fuel injection system, t_d can be considered as the fuel injection pulse width of a single engine period (I_w).

The mean value model of fuel-powered aircraft engine can be analyzed as shown in Fig. 3. Fuel injector sprays fuel into the manifold of the engine in which the fuel flow is expressed by using $\dot{m}_{fi}$. α is opening degree of the throttle plate. In the manifold of the engine, V_m means the manifold volume, P_m is the air pressure, and T_m is the air temperature. The mixed

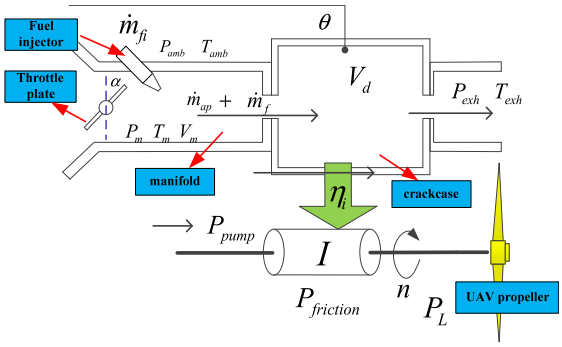

FIGURE 3. Schematic block diagram of the working process of the aircraft engine.

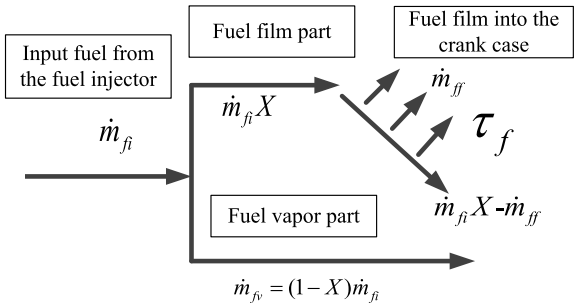

FIGURE 4. Schematic diagram of the fuel film evaporation.

air mass flow and fuel mass flow finally entering into the crack case are expressed by $\dot{m}_{ap}$ and $\dot{m}_i$, respectively. Load of UAV propeller is considered as an engine disturbance, so the total energy of the mixed fuel and air is the input energy, and the output power includes the load power P_L, friction power $P_{friction}$ and pumping loss power P_{pump}. The energy consumption efficiency from fuel to the output is expressed as η_i. θ is advance angle of ignition, V_d is capacity of the engine, P_{amb} and T_{amb} are ambient pressure and temperature, respectively.

The mean value model of the fuel-powered engine includes three subsystems:

As shown in Fig. 4, in the fuel film part, ratio X evaporates dynamically with film evaporation coefficient τ_f.

We can obtain the fuel vapor and fuel film equations as

$$\dot{m}_{fv} = (1 - X)\dot{m}_{fi} \tag{6}$$

$$\dot{m}_{ff} = \frac{1}{\tau_f}(-\dot{m}_{ff} + X\dot{m}_{fi}), \tag{7}$$

and

$$\dot{m}_f = \dot{m}_{fv} + \dot{m}_{ff}, \tag{8}$$

where $\dot{m}_{fv}$ is the mass flow of the fuel vapor into the crank case and $\dot{m}_{ff}$ is the mass flow of the fuel film into the crank case.

An air mass flow in the manifold is dynamically generated by the outside air passing through the throttle plate, and a part of it is pulled into the crank case during the operation of

the engine. The associated equations are as follows:

$$\dot{m}_{man} = \dot{m}_{at} - \dot{m}_{ap}, \tag{9}$$

and

$$\dot{m}_{ap} = nV_d\rho_{man}\eta_{vol}/120, \tag{10}$$

where $\dot{m}_{man}$ is the air mass flow in the manifold of the engine, $\dot{m}_{at}$ is the air mass flow through the throttle plate, ρ_{man} is the density of the air in the manifold, n is the rotating speed of the engine, V_d is the displacement of the engine, and η_{vol} expresses the working volume coefficient of the engine. As in the manifold, $\rho_{man} = P_m/(RT_m)$, where R is the gas constant factor, and so, equation (10) can also be expressed as:

$$\dot{m}_{ap} = nV_dP_m\eta_{vol}/(120RT_m), \tag{11}$$

Recent research [23]–[25] has proved that the working volume coefficient is related with the air pressure in the manifold, and so, equation (11) can also be transformed as follows:

$$\dot{m}_{ap} = nV_d(y_1P_m - y_2)/(120RT_m), \tag{12}$$

where y_1 and y_2 are the air mass flow coefficients, which need to be calibrated based on the results of the aircraft engine experiments. Numerous studies [18]–[23] have been conducted on the input air mass flow through the throttle plate, and it has been concluded that the air mass flow is related with key parameters including air pressure in the manifold P_{man} and throttle opening degree α. The mass flow equation can be written as follows:

$$\dot{m}_{at}(\alpha, p_r) = \frac{P_{amb}}{\sqrt{T_mR}}\beta_1(\alpha)\beta_2(p_r) \tag{13}$$

$$\beta_1(\alpha) = 1 - a_1\cos(\alpha) + a_2\cos^2(\alpha), \tag{14}$$

and

$$\beta_2(p_r) = \begin{cases} \left(\sqrt{p_r^{p_1} - p_r^{p_2}}\right)/p_n, & if\,(p_r \geq p_c) \\ 1, & if\,(p_r < p_c) \end{cases}, \tag{15}$$

where $p_r = P_m/P_{amb}$ is the air pressure ratio of the front and back of the throttle plate and α_1 and α_2 are the coefficients of the air mass flow into the crank case. P_c is expressed as

$$P_c = \left(\frac{p_1}{p_2}\right)^{\left(\frac{1}{p_2-p_1}\right)}, \tag{16}$$

where p_1 and p_2 are related constant dimensionless factors, which are often set as 0.4404 and 2.3143, respectively.

Based on the air state equation, the equation of the air pressure in the manifold can be written as follows:

$$\dot{P}_m = \frac{RT_m}{V_m}(\dot{m}_{at}(\alpha, P_m) - \dot{m}_{ap}(n, P_m)) \tag{17}$$

Based on the principle of conservation of energy, the equations of the crank shaft and load on the engine can be expressed as follows:

$$\dot{n} = -\frac{P_f + P_p + P_b}{In} + \frac{H_u}{In}\eta_i\dot{m}_f, \tag{18}$$

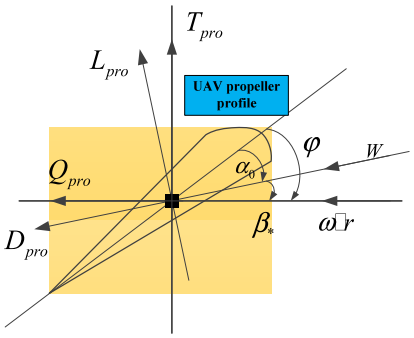

FIGURE 5. Force analysis diagram of a UAV propeller profile.

where P_f is the friction power related with engine speed n, P_p is the pumping loss power related with engine speed n and manifold pressure P_{man}, P_b is the power added on the engine by the loads, H_u is gas calorific value of the fuel, which is 43000 kJ/kg, and I is the inertia of the engine. The power equations are as follows:

$$P_f = (b_1 + b_2n + b_3n^2)n, \tag{19}$$

and

$$P_p = (c_1 + c_2n)P_mn, \tag{20}$$

where b_1, b_2, b_3, c_1, and c_2 are the power coefficients of the engine.

Energy consumption efficiency η_i is related with key parameters of engine speed n, air pressure of manifold P_m, ignition angle θ, and air/fuel ratio λ. The energy consumption efficiency is as follows:

$$\eta_i(\lambda, \theta, n, p) = \eta_n(n)\eta_p(p)\eta_\theta(\theta)\eta_\lambda(\lambda), \tag{21}$$

where $\eta_n(n)$, $\eta_p(p)$, $\eta_\theta(\theta)$, and $\eta_\lambda(\lambda)$ represent the efficiency factors related with the parameters.

Load power of the engine P_b is the output power of the UAV propeller during a typical working process. According to the Blade element theory, the UAV propeller can be divided to numerous elements. Each element is force analyzed, as shown in Fig. 5. The lift force and drag force of each element are analyzed. Finally, the elements are accumulated to obtain the total lift force and drag force of the propeller, and the power of the rotating propeller can be calculated.

The lift and drag forces on the propeller element are as follows:

$$\Delta L_{pro} = \frac{1}{2}C_L\rho_{amb}\,|\vec{v}|^2A_{\Delta r}, \tag{22}$$

and

$$\Delta D_{pro} = \frac{1}{2}C_D\rho_{amb}\,|\vec{v}|^2A_{\Delta r}, \tag{23}$$

where ΔL_{pro} is the lift force on the propeller element, C_L is the propeller lift force coefficient, ρ_{amb} is the density of the ambient air, $\vec{v}$ is the line speed relative to air, and $A_{\Delta r}$ is the surface area of the propeller element. Similarly, ΔD_{pro} is

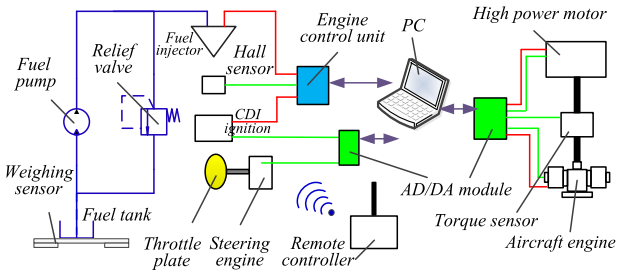

FIGURE 6. Diagram of the experimental station of the fuel-powered aircraft engine.

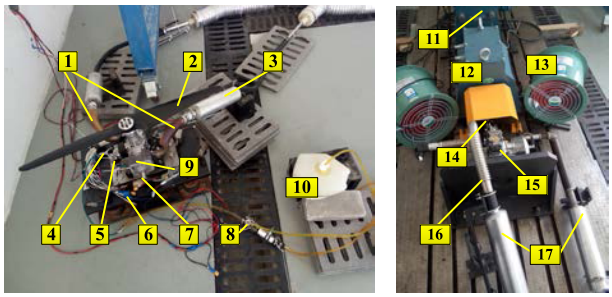

(a) (b)

FIGURE 7. Experimental stations of the fuel-powered aircraft engine (1) exhaust tube, (2) UAV propeller, (3) engine silencer, (4) electronic fuel injector, (5) throttle body, (6) engine control unit, (7) CDI ignition, (8) fuel pump, (9) gas-powered aircraft engine, (10) mini fuel tank, (11) high-power motor, (12) torque sensor, (13) cooling fan, (14) torque sensor, (15) aircraft engine, (16) exhaust tube, and (17) engine silencer.

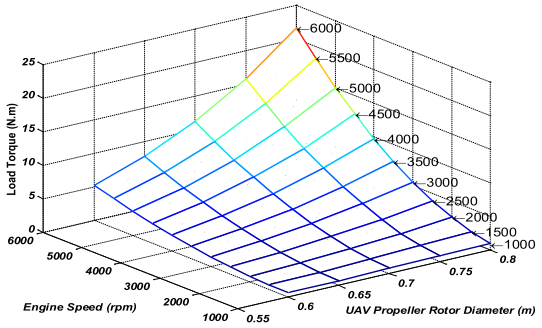

FIGURE 8. Torque of different propellers at different rotating speeds.

the drag force on the propeller element and C_D is the propeller drag force coefficient.

In Fig. 5, the angle between tensile force T_{pro} and lift force L_{pro} is incoming flow angle β_* which is equal to flow incidence angle φ minus airfoil attack angle α_0. Therefore, the tensile and lift forces can be calculated as

$$\Delta T_{pro} = \Delta L_{pro} \cos \beta_* - \Delta D_{pro} \sin \beta_*, \tag{24}$$

and

$$\Delta Q_{pro} = \Delta D_{pro} \cos \beta_* + \Delta L_{pro} \sin \beta_*, \tag{25}$$

therefore, torque of the propeller M_R is

$$M_R = \sum \Delta Q_{pro} r_{pro} = \sum (\Delta D_{pro} \cos \beta_* + \Delta L_{pro} \sin \beta_*) r_{pro} \tag{26}$$

or

$$M_R = Q_{pro} r_{pro} = (D_{pro} \cos \beta_* + L_{pro} \sin \beta_*) r_{pro}, \tag{27}$$

where r_{pro} is the distance between the center points of the hub and propeller. Therefore, load power of the engine P_b can be obtained as:

$$P_b = M_R n = (D_{pro} \cos \beta_* + L_{pro} \sin \beta_*) r_{pro} n \tag{28}$$

IV. EXPERIMENTAL VERIFICATION OF THE MATHEMATICAL MODEL

To verify the above mathematical model, experimental stations of the aircraft engine with the UAV propeller are designed and built as shown in Figs. 6 and 7. The experiments include UAV propeller experiments and power experiments. In the UAV propeller experiments, control parameters such as the fuel injection flow, throttle opening degree, and ignition advanced angle, can be accurately controlled, and the rotating speed of the UAV propeller and oil consumption can be tested. In addition, the engine power experiments are designed to study the power characteristics of the engine. Key parameters of the experimental components are shown in TABLE 1.

TABLE 1. Parameters of the experimental components.

Parameter Name	Value
Inject fuel pulse width	4.0ms
Starting speed	400rpm
Inject fuel angle	25°
Radius of propeller	0.5m
Inject fuel pressure	0.35MPa
Ignition angle	25°
Ratio of gasoline and engine oil	40:1
Engine capacity	170cc

A. UAV PROPELLER EXPERIMENTS

As shown in Figs. 6 and 7 (a), the UAV propeller is installed on the aircraft engine. During the experiments, users can control the engine speed by a remote controller that can control the opening degree of the throttle plate. The data of the engine speed and opening degree of the throttle plate are detected by a data acquisition card on the computer.

To create the same experimental condition of the UAV propeller, the injector fuel pulse width is set as 4 ms and ignition angle is set as 30° before the top dead center position. NACA 0012 airfoil UAV propeller is selected, and we set the propeller design values and drag force coefficients according to U.S. standards [32]. Then, according to equations (22)–(29), the working load of the UAV propeller can be calculated as shown in Fig. 8. Here, we select a propeller with a rotor diameter of 0.8 m.

As can be seen in Fig. 9, the throttle opening degree is set as 20° to smoothly start the aircraft engine, and after 5 s, the throttle is increased to 45°. After approximately 10 s, the throttle is again reduced to 20°. To simulate the same

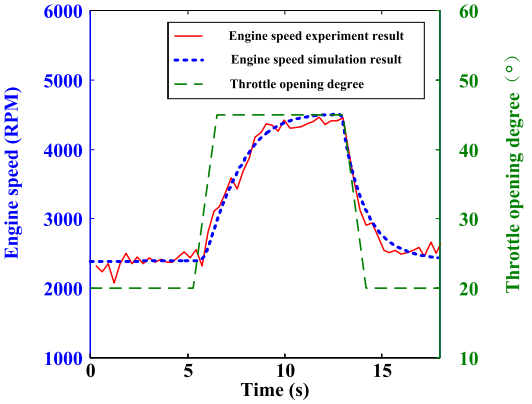

FIGURE 9. Simulation and experiment curves of the aircraft engine speed.

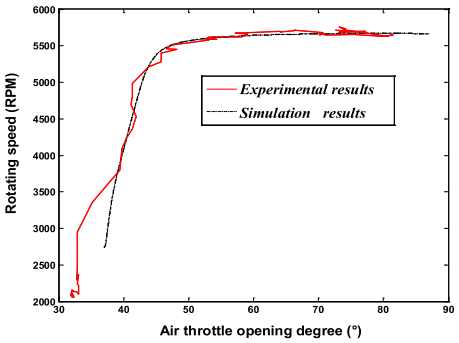

FIGURE 10. Engine speed curves when the throttle opening degree is increased.

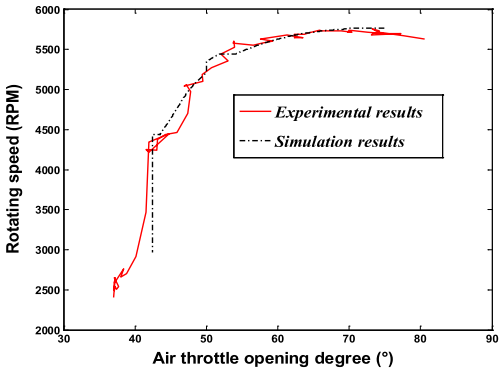

FIGURE 11. Engine speed curves when the throttle opening degree is decreased.

working condition, in the simulation, the throttle is set at the same degree. The simulation and experiment results are in good agreement, validating that the engine speed model is effective.

To simulate all the real working conditions of a fuel-powered aircraft engine, the throttle opening degree is increased from the lowest to largest value and then reduced to zero. The working speeds of the corresponding throttle opening degrees so obtained as displayed in Figs. 10 and 11. Then, the error in the engine speed is obtained as depicted in Fig. 12, according to equation (29).

$$e_n = \left| n_{\exp} - n_{sim} \right| / n_{\exp}, \tag{29}$$

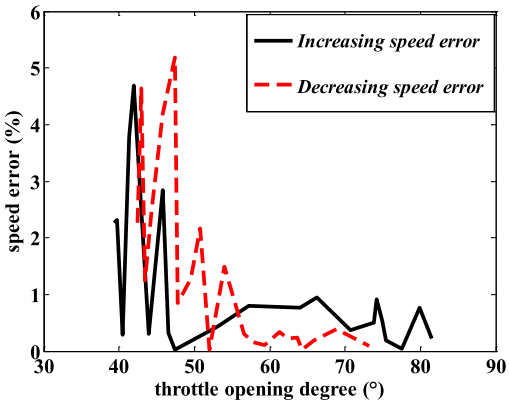

FIGURE 12. Engine speed error when increasing and decreasing the throttle opening degree.

where e_n is the error in the engine speed and n_{exp} and n_{sim} are the speed values from the experiment and simulation, respectively.

If we calculate the absolute value of the difference between the two curves, we can obtain the engine model error. As displayed in Figs. 10 and 11, the simulation results are consistent with the experimental results, which verifies the validity of the above mathematical model. Figure 12 shows that the highest engine speed error is less than 5% when the throttle angle is approximately 45°. When the air–fuel mixture is temporarily decreased, the engine starts with a high initial acceleration. Consequently, at first, the curves of the experimental results slightly deviate from the simulation curves. Moreover, there are clear distinctions between the curves produced in the increasing and decreasing processes. These are because the engine speed is mainly affected by the present engine speed, air–fuel mixture concentration, and working condition of the propeller. In addition, the curves correspond to the same maximum speed, and when the throttle plate degree is higher than approximately 55°, the engine speed almost stops increasing. This is because the maximum speed is limited by the structure and type features of the aircraft engine.

B. OUTPUT POWER EXPERIMENTS

As depicted in Figs. 6 and 7(b), in the output power experiments, the UAV propeller is uninstalled and a torque sensor and high-power motor are rigidly connected to the engine output shaft. The torque sensor can real-time measure the output torque of the engine, and then the output power of the aircraft engine can be calculated according to the real-time engine speed.

First, the motor drags the engine to rotate. When the engine is started and the speed becomes higher than the motor start speed, the motor provides a controllable load to simulate the propeller load. In the experiments, the throttle opening angle is set up constantly, and the load on the engine is gradually added. The engine speed changes with the variation in the output torque. When the engine speed is stable,

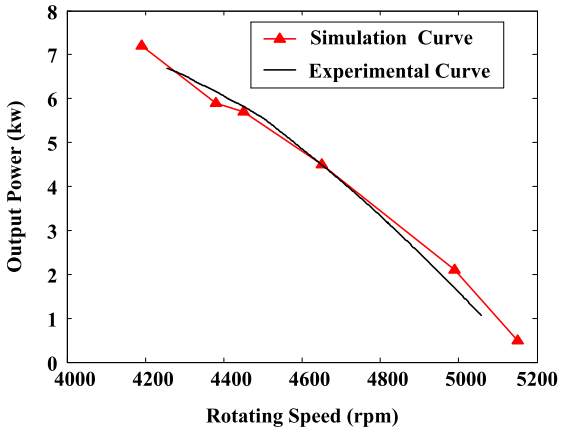

FIGURE 13. Engine output power when the rotating speed is decreased.

the corresponding value of the output power is recorded. All the results are averaged to ensure the accuracy. On the basis of previous research [33], in the mean value model of the fuel-powered engine, the output torque (T_{out}) can be calculated from the following equation:

$$T_{out} = M_a(\mathrm{d}_0 + \mathrm{d}_1\theta + \mathrm{d}_2\theta^2) + (\mathrm{e}_0 + \mathrm{e}_1\theta + \mathrm{e}_2\theta^2) + (\mathrm{f}_0 + \mathrm{f}_1\lambda + \mathrm{f}_2\lambda^2) + (\mathrm{g}_0 + \mathrm{g}_1 n + \mathrm{g}_2\mathrm{n}^2) + \mathrm{h}_0 n\theta \tag{30}$$

where M_a is the mixture quality of the intake air and fuel of engine and d_0, d_1, d_2, e_0, e_1, e_2, f_0, f_1, f_2, g_0, g_1, g_2, and h_0 are the parameter coefficients of the output torque. The coefficients of the output torque are obtained from the parameter calibrations based on the experiment results, and we can obtain the dynamic output torque from the simulations. However, for accuracy, the simulation results are also averaged. Based on the results in Figs. 10 and 11, the ranges of the engine speed and throttle opening degree are set as 4000 rpm to 5500 rpm and 35° to 55°, respectively. Next, the results of the output power is obtained as displayed in Fig. 13.

From Fig. 13, the simulation curve is consistent with the experimental results after the parameter fitting. In addition, the output power of the engine decreases with the increase in the engine rotating speed. This is because at first the engine is started with a low load torque, and its speed is up to approximately 6000 rpm, which is the highest value. Then, a load torque is gradually added, and the engine speed is reduced. However, when the load torque is added, the resistance of the engine pistons will increase, and air pressure in the engine cylinder will also enhance. This will enhance the combustion process, and the output power of the engine will also increase.

Uncertainty parameters of the experiments mainly include calibration coefficients of the output power. The uncertain factors mainly come from the mechanical friction, fuel burning performances affected by the ambient temperature and humidity and so on. However, considering the uncertainty of the calibration relationship among the output power, air fuel ratio and the engine speed, uncertainty of the output power is only regarded, and the uncertainty range of the output power factor (compared with the original experiment calibration result) is settled to 0.8∼1.2.

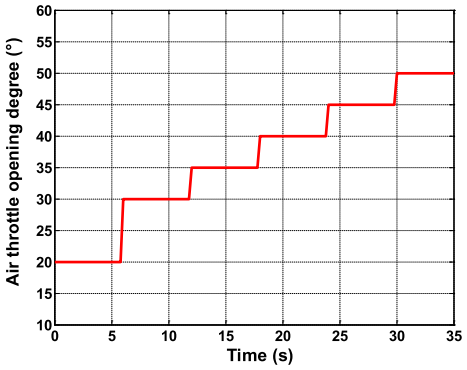

FIGURE 14. Setting diagram of the throttle opening degree.

V. STUDY ON POWER CHARACTERISTICS OF FUEL-CONTROLLED AIRCRAFT ENGINE

Enhancement of the aircraft engine power characteristics will reduce the energy consumption during engine operation, and then extend the cruising duration of the UAV. In this research, the effects of key parameters on the main engine power characteristics are analyzed based on the simulation results using the above mathematical model.

According to the analysis results, the working characteristics of the fuel-controlled aircraft engine are mainly affected by the throttle opening degree (α), fuel injection pulse width (I_w), advance angle of ignition (θ), fuel injection delay width (D_w), and rotor diameter of the UAV propeller (D_{pro}). In the study, to illustrate the effect of the parameters on the power characteristics, each parameter is varied for comparison, whereas the other parameters are kept constant.

The researched characteristics of the aircraft engine mainly consist of the engine speed (n) and output power (P_{out}). In addition, another important attribute to evaluate the fuel utilization [34]–[37] is the power efficiency of the aircraft engine (η_e),calculated by the following equation:

$$\eta_e = \frac{P_{out}}{P_{in}} = \frac{nT_{out}}{9550\dot{m}_{fi}H_u}, \tag{31}$$

where P_{in} is the input power converted from the injected fuel mass flow. UAV driver controls the propeller rotating speed by remote controlling the throttle opening degree. So in the simulation, the different engine working conditions are directly obtained by setting different throttle opening degree values. According to the practical application of UAV, throttle opening degree is step-type set as shown in Fig. 14. Several latest articles have analyzed the engine optimization method based on the dynamic model [38], [39]. According to Figs. 10 and 11, range of the throttle opening degree is 20 to 50 degrees. Time interval between each opening degree step is about 5 seconds to ensure the engine to reach steady state. In each parameter study, the speed, output power and air/fuel

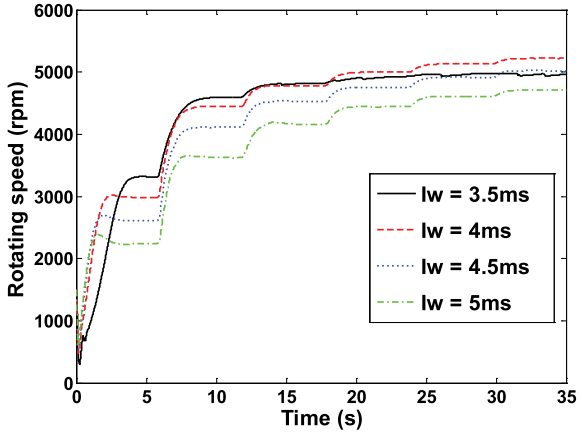

FIGURE 15. Rotating speed curves of the aircraft engine.

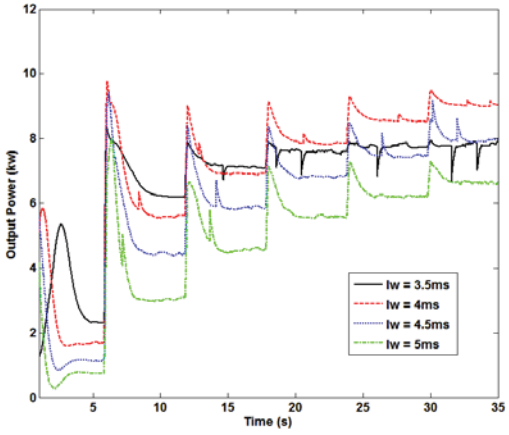

FIGURE 16. Dynamic output power curves of the aircraft engine.

ratio are researched dynamically. Moreover, average values of output power and power efficiency of engine are taken to analyze the influences of the key parameters under different working conditions. Then we get the results as follows.

A. EFFECT OF FUEL INJECTION PULSE WIDTH (I_W) ON OUTPUT CHARACTERISTICS

The fuel injection pulse width is directly controlled by the ECU unit, and it directly controls the fuel injection flow of the engine. When the advance angle of ignition (θ) is set as 20°, the fuel injection delay width (D_w) is set as 0.5 ms, rotor diameter of the UAV propeller (D_{pro}) is selected as 0.8 m, and fuel injection pulse width (I_w) is set as 3.5, 4, 4.5, and 5 ms. Then the output characteristics are studied.

Fig. 15 depicts the variation trends of the dynamic rotating speed of the aircraft engine. The speed curves have an increasing ladder shape with the increase in the settled throttle opening degree. Moreover, overall, the speed curves are lower for a larger fuel injection pulse width (I_w), but the top speed of the engine is the highest when I_w is 4 ms. This is because when I_w is higher than 4 ms, the injected fuel in the manifold is too large, and the air–fuel mixture cannot sufficiently burn.

As is shown in Fig. 16, the engine output power is affected by the fuel injection pulse width. First, when the throttle opening degree is varied from 20° to 30°, the output power rapidly increases from approximately 2 kW to 8 kW, but when the engine speed becomes stable, the output power gradually reduces to approximately 6 kW and then becomes steady. This is because when the throttle opening is larger, the engine accelerates and the air pressure between the manifold and cylinder chambers increases, increasing the air intake mass flow, and thereby, increasing the output power. When the opening degree and engine speed are stable, the output power decreases slightly. In addition, the overall output power increases and then reduces significantly with the increase in the fuel injection pulse width, and when P_w is approximately 4 ms, the average output power is the highest.

Variation trend of the power efficiency under the effect of the fuel injection pulse width at different engine speeds is

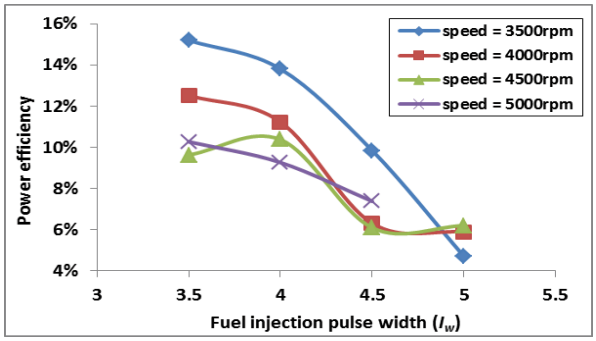

FIGURE 17. Power efficiency curves of the aircraft engine.

through the study from Fig. 17. It can be concluded that when the engine speed is increased from 3500 rpm to 5000 rpm, the power efficiency reduces by approximately 5%. Furthermore, the power efficiency decreases by 5%–10%, with an increase in the fuel injection pulse width from 3.5 ms–5 ms. This is because when P_w is set higher, fuel intake is higher; however, the output power is lower. In addition, when the engine operates at a high speed, the engine is close to the speed and power limit, but the fuel consumption is much higher. From the figures, the appropriate fuel injection pulse width is 3.5 ms–4.0 ms to ensure the output power and power efficiency.

B. EFFECT OF ADVANCE ANGLE OF IGNITION (θ) ON OUTPUT CHARACTERISTICS

The advance angle of ignition (θ) determines the piston position of the engine cylinder when a spark is triggered. Different advance angles of ignition lead to different volumes of the cylinder chamber and different pressures of the compressed mixture of the air and fuel. When the fuel injection pulse width (P_w) is set as 4 ms, the fuel injection delay width (D_w) is set as 0.5 ms, the rotor diameter of the UAV propeller (D_{pro}) is chosen as 0.8 m, and advance angle of ignition (θ) is set as 10, 20, 30, 40, and 50°. The following output characteristics are examined.

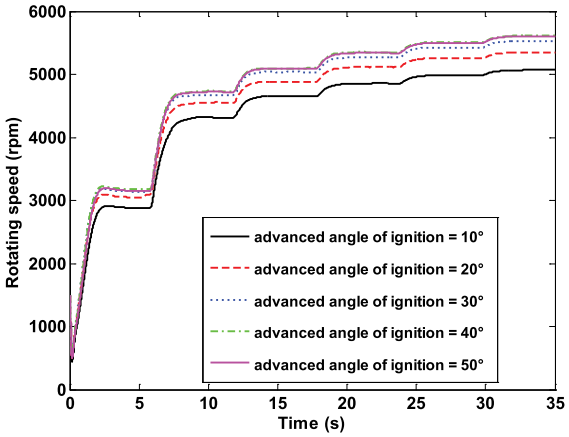

FIGURE 18. Rotating speed curves of the aircraft engine.

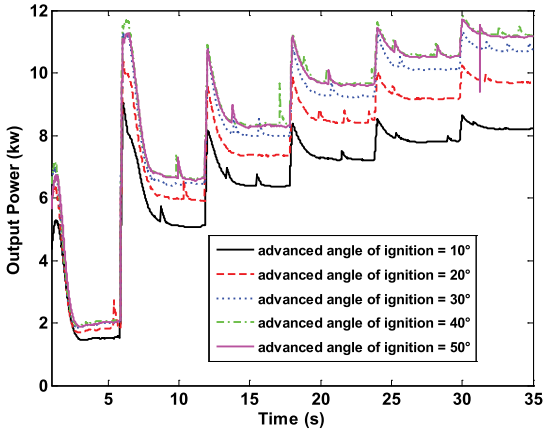

FIGURE 19. Dynamic output power curves of the aircraft engine.

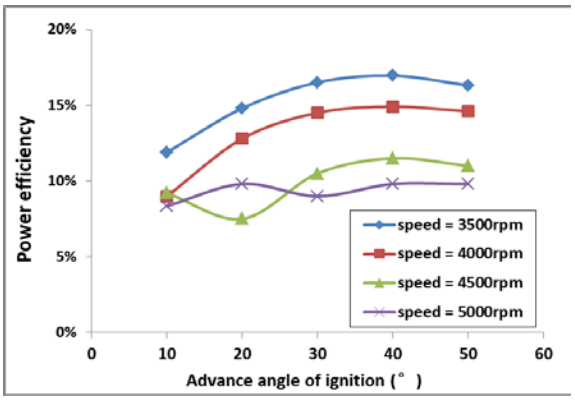

FIGURE 20. Power efficiency curves of the aircraft engine.

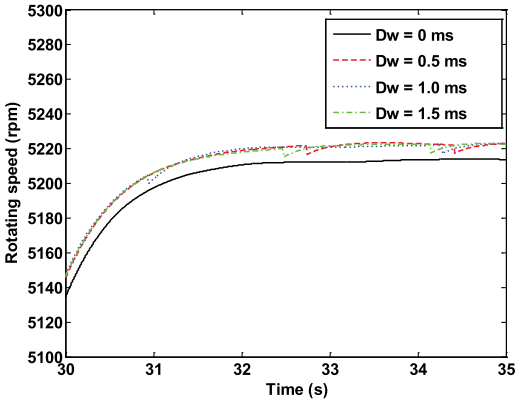

FIGURE 21. Rotating speed curves of the aircraft engine.

As shown in Fig. 18, the advance angle of ignition can deeply affect the engine speed. When the advanced angle of ignition is set larger, the rotating speed increases, but when θ is higher than 40 degrees, the engine speed will be smaller. That is because when the advance angle of ignition is set too high, the distance between piston and the top dead center is too far, and the pressure of the engine chambers is not high enough for further acceleration. In Fig. 19, the whole trend of the output power curves is similar to that of the rotating speed. The increase of advanced angle of ignition with a limit of 40 degrees will lead to the rise of the output power.

From Fig. 20, at speeds from 3500 rpm to 4500 rpm, as the advance angle of ignition increases, the power efficiency curve increases and then decreases. When θ is approximately 40°, the power efficiency is maximum and over 15%. Furthermore, increasing the advance angle of ignition from 10° to 40° increases the power efficiency by 5%. However, at the speed of 5000 rpm, the power efficiency decreases and is not apparently affected by the advance angle of ignition. Therefore, we should choose an appropriate θ at different speeds by analyzing the results to obtain the highest output power and power efficiency.

C. EFFECT OF FUEL INJECTION DELAY WIDTH (D_W) ON OUTPUT CHARACTERISTICS

The fuel injection delay width (D_w) controls the start time of the fuel injection. The fuel injection delay width is usually set to coordinate the times of the fuel injection and ignition. When the fuel injection pulse width (P_w) is set as 4 ms, the advance angle of ignition (θ) is set as 20°, rotor diameter of the UAV propeller (D_{pro}) is chosen as 0.8 m, and fuel injection delay width (D_w) is set as 0, 0.5, 1, and 1.5 ms. The following results of the output characteristics are obtained.

Figs. 21 and 22 exhibit the dynamic characteristics of engine speed and output power that are affected by the fuel injection delay width. The fuel injection delay width has a less impact on the engine rotating speed and output power. The reason is that the injection delay width mainly controls the fuel injection time. However, when the fuel is injected into the manifold of the engine, the fuel and air will immediately mix, and the fuel flow will not be significantly affected by the delayed injected fuel. However, from Figs. 20 and 21, when D_w is set lower, the curves of the engine speed and output power become smoother without an apparent decrease.

In Fig. 23, when the fuel injection delay width increases from 0.5 mm to 1.5 mm at an engine speed of 3500 rpm–4000 rpm, the power efficiency is improved by 6%.

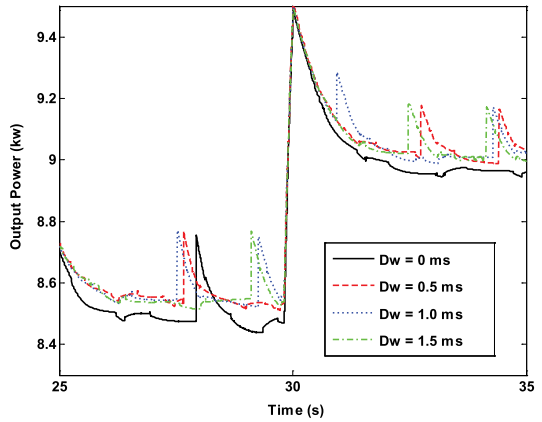

FIGURE 22. Dynamic output power curves of the aircraft engine.

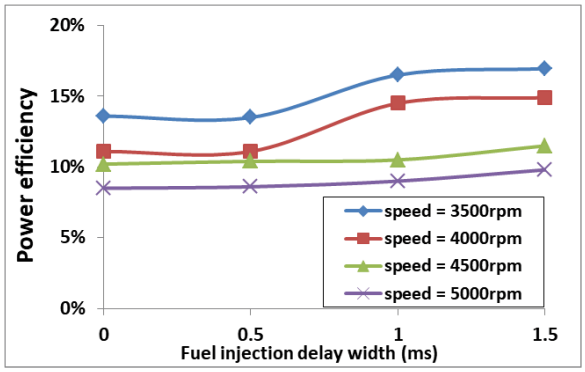

FIGURE 23. Power efficiency curves of the aircraft engine.

At a speed of over 4000 rpm, the fuel injection delay width does not apparently affect the power efficiency. The reason is that when the engine speed is relatively low, the injected fuel mass flow is easily affected, and the fuel injection delay width provides sufficient time for the vaporization of the fuel film. However, when the engine speed is sufficiently high, the effect on the fuel mass flow can be neglected. Therefore, according to the analysis results, the fuel injection delay width can be set between 0.5 ms and 1 ms to ensure the dynamic stability and efficiency at a low speed.

D. EFFECT OF PROPELLER ROTOR DIAMETER (D_{PRO}) ON OUTPUT CHARACTERISTICS

As shown in Fig. 8, the rotor diameter of the UAV propeller (D_{pro}) affects the load torque on the engine under different working conditions, and the load torque then affects the output characteristics of the operating aircraft engine. The fuel injection delay width (D_w) controls the start time of the fuel injection. When the fuel injection pulse width (P_w) is set as 4 ms, the advance angle of ignition (θ) is set as 20°, fuel injection delay width (D_w) is set as 0.5 ms, rotor diameter of the UAV propeller (D_{pro}) is set as 0.65, 0.7, 0.75, and 0.8 m, and shape of the UAV propeller is follows the NACA 0012 standard.

As is shown in Figs. 24 and 25, when the rotor diameter of the UAV propeller (D_{pro}) is large, the engine speed reduces,

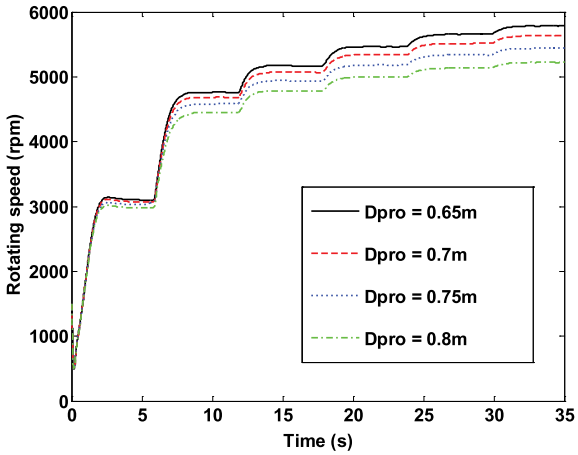

FIGURE 24. Rotating speed curves of the aircraft engine.

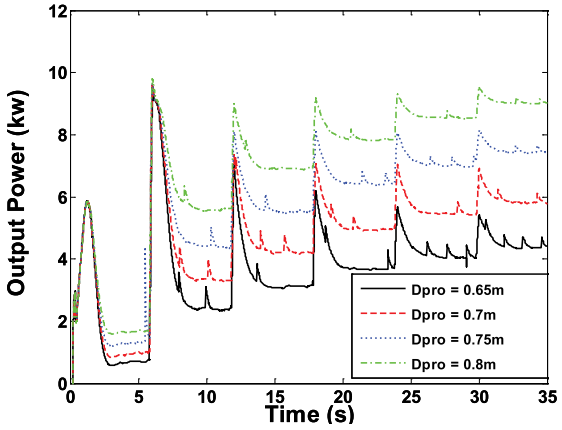

FIGURE 25. Dynamic output power curves of the aircraft engine.

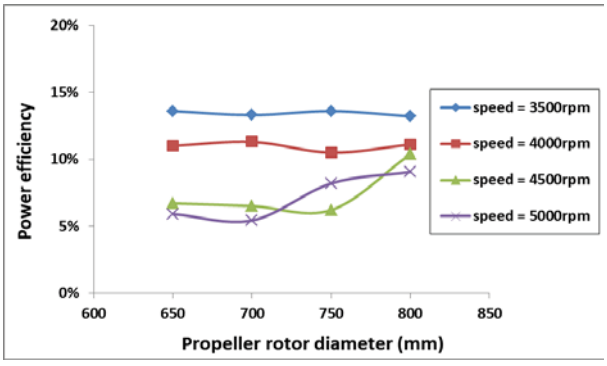

FIGURE 26. Power efficiency curves of the aircraft engine.

whereas the output power increases. Furthermore, the variation extent of the output power is much higher than that of the rotating speed. The larger D_{pro} at the same speed, the load torque of the engine is much higher, as shown in Fig. 8.

As is depicted in Fig. 26, when the engine speed is from 3500 rpm to 4000 rpm, the propeller rotor diameter has a negligible effect on the power efficiency. However, when the engine speed is higher than 4000 rpm, increasing the propeller rotor diameter from 650 mm to 800 mm increases the power

TABLE 2. Endurance improvement results.

Engine Speed	Original Endurance	Improved Endurance	Improved percentage
4000rpm	2h20min	2h55min	25%
4500rpm	2h04min	2h26min	16.8%
5000rpm	1h43min	2h02min	18.4%
5500rpm	1h21min	1h33min	14.8%
6000rpm	1h05min	1h11min	9.2%

efficiency of the aircraft engine by approximately 5%. The reason is that when the speed is higher, the resistance moment is also increased, which in turn increases the pressure of the cylinder chambers. Consequently, when the engine speed is higher than 4000 rpm, a propeller with a larger rotor diameter is more suitable for the enhancing the power efficiency.

Compared with the published literature [38], [39], more control parameters are discussed, and the affecting rules are analyzed. This paper overall considers the fuel injection delay width, the advance angle of ignition, and the fuel injection delay width. In addition, different engine speeds correspond to different optimal combination of injection parameters. Moreover, method type in this paper belongs to discussion of the open-loop calibration of the calibration, and the other published literatures are mainly concentrated on the control algorithms. Therefore, method in this paper is more practical.

E. IMPROVEMENT RESULT OF UAV FLIGHT ENDURANCE

Experiments of the aircraft engine are carried out in which the optimized method is applied in order to analyze the improvement result. In the experiments the fuel flow is measured under different engine working speeds, and the prolonged endurance of the fuel-powered UAV is calculated. Then the results are shown as the following table. In the comparison, the original control parameters are settled as follows: the fuel injection pulse width is set to 4.5 ms, the advance angle of ignition is set to 10°, and the fuel injection delay width is set to 0 ms; furthermore, the improved parameters are: the fuel injection pulse width is set to 4.2 ms, the advance angle of ignition is set to 25°, and the fuel injection delay width is set to 0.5 ms. Then the endurance of the DZ310 UAV is calculated according to the fuel capacity (3∼4L) and the fuel consumption rate at different engine working speeds.

As can be seen in TABLE 2, the endurance can be prolonged by improving the control parameters of the fuel injection system according to the analyzing results. The common applied engine speed is 4500 to 5500 rpm. According to the calculation results, the endurance can be prolonged by about 15% to 18%. And that is correspond to the analyzing results.

VI. CONCLUSION

In this study, to improve the flight duration and power efficiency of a UAV, the power characteristic studies of a fuel-controlled aircraft engine for a fuel-powered UAV is conducted. The mathematical model of the aircraft engine is built and verified experimentally. Furthermore, the effects of key parameters including the fuel injection pulse width, advance angle of ignition, fuel injection delay width, and rotor diameter of the UAV propeller, on the engine power characteristics are examined. The following conclusions can be drawn:

(1).The comparison of the simulation outputs with the experimental data shows that they are in good agreement, which verifies the effectiveness of the mathematical model;

(2).Based on the simulation analysis of the characteristics at different throttle opening degrees, increasing the rotating speed from 3500 rpm to 5000 rpm decreases the power efficiency of the aircraft engine by 5% to 10% under different conditions. To achieve the highest power efficiency in a typical operating situation, the application speed should be 3500 rpm–4000 rpm;

(3).Reducing the fuel injection pulse width from 5 ms to 3.5 ms increases the power efficiency by 10%. Moreover, increasing the advance angle of ignition from 10° to 40° improves the power efficiency by 5%. However, reducing the fuel injection pulse width to below 3.5 ms or increasing the advance angle of ignition beyond 40° leads to insufficient output power;

(4).When the fuel injection delay width increases from 0.5 mm to 1.5 mm at the engine speed of 3500 rpm–4000 rpm, the power efficiency is improved by 6%. In addition, when the engine speed is higher than 4000 rpm, increasing the propeller rotor diameter from 650 mm to 800 mm enhances the power efficiency of the aircraft engine by approximately 5%. Therefore, when the engine speed is higher than 4000 rpm, to choose a propeller of a larger rotor diameter is more suitable.

(5). According to several comparison experiments, the endurance can be prolonged by about 15% to 18% under the common applied engine speed.

This research can provide a reference for updating the fuel characteristic of aircraft engine and prolonging the cruising duration of fuel-powered UAV.

REFERENCES

[1] C. Stöcker, R. Bennett, F. Nex, M. Gerke, and J. Zevenbergen, "Review of the current state of UAV regulations," *Remote Sens.*, vol. 9, no. 5, pp. 459–484, May 2017.
[2] C. H. Hugenholtz, B. J. Moorman, K. Riddell, and K. Whitehead, "Small unmanned aircraft systems for remote sensing and earth science research," *Eos, Trans. Amer. Geophys. Union*, vol. 93, no. 25, p. 236, Jun. 2012.
[3] C. Zhang and J. M. Kovacs, "The application of small unmanned aerial systems for precision agriculture: A review," *Precis. Agricult.*, vol. 13, no. 6, pp. 693–712, Dec. 2012.
[4] E. A. Hinkley and T. Zajkowski, "USDA forest service–NASA: Unmanned aerial systems demonstrations–pushing the leading edge in fire mapping," *Geocarto Int.*, vol. 26, no. 2, pp. 103–111, Feb. 2011.
[5] T. Liu, X. Hu, S. E. Li, and D. Cao, "Reinforcement learning optimized look-ahead energy management of a parallel hybrid electric vehicle," *IEEE/ASME Trans. Mechatronics*, vol. 22, no. 4, pp. 1497–1507, Aug. 2017.
[6] T. Donateo, A. Ficarella, L. Spedicato, A. Arista, and M. Ferraro, "A new approach to calculating endurance in electric flight and comparing fuel cells and batteries," *Appl. Energy*, vol. 187, no. 1, pp. 807–819, Feb. 2017.
[7] A. C. Marta and P. Gamboa, "Long endurance electric UAV for civilian surveillance missions," in *Proc. St. Petersburg, 29th Int. Council Aeronaut. Sci.*, Sep. 2014, pp. 1–19.

[8] M. Bogarra, J. M. Herreros, A. Tsolakis, A. P. E. York, P. J. Millington, and F. J. Martos, "Impact of exhaust gas fuel reforming and exhaust gas recirculation on particulate matter morphology in gasoline direct injection engine," *J. Aerosol Sci.*, vol. 103, pp. 1–14, Jan. 2017.
[9] K. Han, E. Lee, M. Choi, and S. B. Choi, "Adaptive scheme for the real-time estimation of tire-road friction coefficient and vehicle velocity," *IEEE/ASME Trans. Mechatronics*, vol. 22, no. 4, pp. 1508–1518, Aug. 2017.
[10] M. Bogarra, J. M. Herreros, A. Tsolakis, A. P. E. York, and P. J. Millington, "Study of particulate matter and gaseous emissions in gasoline direct injection engine using on-board exhaust gas fuel reforming," *Appl. Energy*, vol. 180, no. 15, pp. 245–255, Oct. 2016.
[11] Y. Jiang, T. Li, and L. Wang, "Novel method for designing high precision parallel kinematic machines based on the smart structure," *IEEE/ASME Trans. Mechatronics*, vol. 22, no. 4, pp. 1899–1902, Aug. 2017.
[12] Y. Chen and R. Raine, "The effects of hydrogen supplementation on idle performance and emissions of an SI engine," in *Proc. Asia Pacific Conf. Combustion*, Jul. 2015, pp. 190–199.
[13] B. Lu, Q. Yu, X. Fu, Y. Shi, and M. Cai, "Parameter matching of hybrid coaxial rotors and multi-rotor UAV's power system," in *Proc. IEEE Int. Conf. Aircraft Utility Syst. (AUS)*, Oct. 2016, pp. 1099–1104.
[14] P. Hooper, "Experimental experience of cold starting a spark ignition UAV engine using low volatility fuel," *Aircr. Eng. Aerosp. Technol.*, vol. 89, no. 1, pp. 106–111, Jan. 2017.
[15] P. Hooper, P. Hooper, T. Al-Shemmeri, and T. Al-Shemmeri, "Improved efficiency of an unmanned air vehicle IC engine using computational modelling and experimental verification," *Aircr. Eng. Aerosp. Technol.*, vol. 89, no. 1, pp. 184–192, Jan. 2017.
[16] H. Bayındır, M. Z. Işık, and H. Aydın, "Evaluation of combustion, performance and emission indicators of canola oil-kerosene blends in a power generator diesel engine," *Appl. Therm. Eng.*, vol. 114, no. 5, pp. 234–244, Mar. 2017.
[17] P. Dubey and R. Gupta, "Effects of dual bio-fuel (Jatropha biodiesel and turpentine oil) on a single cylinder naturally aspirated diesel engine without EGR," *Appl. Therm. Eng.*, vol. 115, no. 25, pp. 1137–1147, Mar. 2017.
[18] M. Müller, E. Hendricks, and S. C. Sorenson, "Mean value modelling of turbocharged spark ignition engines," SAE Tech. Paper 980784, Feb. 1998. doi: 10.4271/980784.
[19] E. Hendricks and S. C. Sorenson, "Mean value modelling of spark ignition engines," SAE Tech. Paper 900616, Feb. 1990. doi: 10.4271/900616.
[20] A. Chevalier, M. Müller, and E. Hendricks, "On the validity of mean value engine models during transient operation," SAE Tech. Paper 2000-01-1261, Mar. 2000. doi: 10.4271/2000-01-1261.
[21] J. van Leersum, "A numerical model of a high performance two-stroke engine," *Appl. Numer. Math.*, vol. 27, no. 1, pp. 83–108, May 1998.
[22] T. Donateo, L. Spedicato, G. Trullo, A. P. Carlucci, and A. Ficarella, "Sizing and simulation of a piston-prop UAV," *Energy Procedia*, vol. 82, pp. 119–124, Dec. 2015.
[23] L. Eriksson, "Modeling and control of turbocharged SI and DI engines," *Oil Gas Sci. Technol.*, vol. 62, no. 4, pp. 523–538, 2007.
[24] S. Watechagit and K. Srinivasan, "Online estimation of operating variables for stepped automatic transmissions," in *Proc. IEEE Conf. Control Appl.*, vol. 1, Jun. 2003, pp. 279–284.
[25] C. Manzie, M. Palaniswami, D. Ralph, H. Watson, and X. Yi, "Model predictive control of a fuel injection system with a radial basis function network observer," *J. Dyn. Syst., Meas., Control*, vol. 124, no. 4, pp. 648–658, Dec. 2002.
[26] L. Cui, T. Wang, K. Sun, Z. Lu, Z. Che, and Y. Sun, "Numerical analysis of the steady-state scavenging flow characteristics of a two-stroke marine engine," SAE Tech. Paper 2017-01-0558, Mar. 2017. doi: 10.4271/2017-01-0558.
[27] A. Santamaria-Navarro, P. Grosch, V. Lippiello, J. Solá, and J. Andrade-Cetto, "Uncalibrated visual servo for unmanned aerial manipulation," *IEEE/ASME Trans. Mechatronics*, vol. 22, no. 4, pp. 1610–1621, Aug. 2017.
[28] Y. Lu and D. B. Olsen, "Optimization method and simulation study of a diesel engine using full variable valve motions," *J. Eng. Gas Turbines Power*, vol. 139, no. 7, pp. 072804-1–072804-8, Jul. 2017.
[29] A. M. Shamekhi and A. H. Shamekhi, "A new approach in improvement of mean value models for spark ignition engines using neural networks," *Expert Syst. Appl.*, vol. 42, no. 12, pp. 5192–5218, Jul. 2015.
[30] T. Broomhead, C. Manzie, M. Brear, and P. Hield, "Model reduction of diesel mean value engine models," SAE Tech. Paper 2015-01-1248, Apr. 2015. doi: 10.4271/2015-01-1248.
[31] K. Nikzadfar and A. H. Shamekhi, "An extended mean value model (EMVM) for control-oriented modeling of diesel engines transient performance and emissions," *Fuel*, vol. 154, no. 15, pp. 275–292, Aug. 2015.
[32] B. Saha, E. Koshimoto, C. C. Quach, E. F. Hogge, T. H. Strom, B. L. Hill, S. L. Vazquez, and K. Goebel, "Battery health management system for electric UAVs," in *Proc. IEEE Aerosp. Conf.*, Mar. 2011, pp. 1–9.
[33] B. Y. Shi and Y. X. Zhang, "The modeling and simulation of torque based on MVEM," *Mech. Eng.*, vol. 2, no. 26, pp. 51–53, Feb. 2010.
[34] J. Na, G. Herrmann, C. Rames, R. Burke, and C. Brace, "Air-fuel-ratio control of engine system with unknown input observer," in *Proc. UKACC 11th Int. Conf. Control (CONTROL)*, Aug. 2016, pp. 1–6.
[35] M. Kumar and T. Shen, "In-cylinder pressure-based air-fuel ratio control for lean burn operation mode of SI engines," *Energy*, vol. 120, no. 1, pp. 106–116, Feb. 2017.
[36] J. W. Gao, Y. H. Zhang, and T. L. Shen, "An on-board calibration scheme for map-based combustion phase control of spark-ignition engines," *IEEE/ASME Trans. Mechatron.*, vol. 22, no. 4, pp. 1485–1496, Aug. 2017.
[37] K. M. Lee, L. Yang, K. Bai, and J. Ji, "An efficient flexible division algorithm for predicting temperature-fields of mechatronic system with manufacturing applications," *IEEE/ASME Trans. Mechatronics*, vol. 22, no. 4, pp. 1818–1827, Aug. 2017.
[38] Y. Wang, Y. Shi, M. Cai, W. Xu, and Q. Yu, "Optimization of air–fuel ratio control of fuel-powered UAV engine using adaptive fuzzy-PID," *J. Franklin Inst.*, vol. 355, no. 17, pp. 8554–8575, 2018.
[39] Y. Wang, Y. Shi, M. Cai, W. Xu, and Q. Yu, "Efficiency optimized fuel supply strategy of aircraft engine based on air-fuel ratio control," *Chin. J. Aeronaut.*, vol. 32, no. 2, pp. 489–498, 2019.

YIXUAN WANG received the B.E. degree from the School of Automation Science and Electrical Engineering, Beihang University, in 2015, where he is currently pursuing the Ph.D. degree. His research interests include fuel and power systems of UAV, fluid control, measurement, and control systems.

YAN SHI received the Ph.D. degree in mechanical engineering from Beihang University, where he is currently an Associate Professor with the School of Automation Science and Electrical Engineering. His research interests include intelligent medical devices and energy-saving technologies of pneumatic systems.

MAOLIN CAI received the Ph.D. degree from the Tokyo Institute of Technology. He is currently a Professor with the School of Automation Science and Electrical Engineering, Beihang University, Beijing, China. His research interests include intelligent medical devices, research on the technology of high efficiency and large scale compressed air energy storage, and so on.

WEIQING XU received the Ph.D. degree in mechanical engineering from Beihang University, where he is currently a Lecturer with the School of Automation Science and Electrical Engineering. His research interests include intelligent mechanical devices and high efficient compressed air energy storage technologies.

TIANYU PAN is currently an Associate Professor with the School of Energy and Power Engineering, Beihang University, Beijing, China. His major research interests include aircraft engine stability study and pneumatic fluid science.

QIHUI YU is currently a Lecturer with the Department of the School of Mechanical Engineering, Inner Mongolia University of Science and Technology. His major research interests include control system of UAV aircraft engine, pneumatic control systems, energy conversion systems, and air-powered vehicles.